# Density functional theory study of the structural and electronic properties of amorphous silicon nitrides: $Si_3N_{4-x}$:H

L. E. Hintzsche,[1] C. M. Fang,[1] T. Watts,[1] M. Marsman,[1] G. Jordan,[1] M. W. P. E. Lamers,[2] A. W. Weeber,[2] and G. Kresse[1]
[1]*University of Vienna, Faculty of Physics and Center for Computational Materials Science, Sensengasse 8/12, A-1090 Vienna, Austria*
[2]*ECN Solar Energy, P.O. Box 1, 1755 ZG Petten, Netherlands*
(Received 2 October 2012; published 14 December 2012)

We present *ab initio* density functional theory studies for stoichiometric as well as nonstoichiometric amorphous silicon nitride, varying the stoichiometry between $Si_3N_{4.5}$ and $Si_3N_3$. Stoichiometric amorphous $Si_3N_4$ possesses the same local structure as crystalline $Si_3N_4$, with Si being fourfold coordinated and N being threefold coordinated. Only few Si-Si and N-N bonds and other defects are found in stoichiometric silicon nitride, and the electronic properties are very similar to the crystalline bulk. In over-stoichiometric $Si_3N_{4+x}$, the additional N results in N-N bonds, whereas in under-stoichiometric $Si_3N_{4-x}$ the number of homopolar Si-Si bonds increases with decreasing N content. Analysis of the structure factor and the local coordination of the Si atoms indicates a slight tendency towards Si clustering, although at the investigated stoichiometries, phase separation is not observed. In the electronic properties, the conduction-band minimum is dominated by Si states, whereas the valence-band maximum is made up by lone pair N states. Towards Si rich samples, the character of the valence-band maximum becomes dominated by Si states corresponding to Si-Si bonding linear combinations. Adding small amounts of hydrogen, as typically used in passivating layers of photovoltaic devices, has essentially no impact on the overall structural and electronic properties.

DOI: 10.1103/PhysRevB.86.235204 PACS number(s): 71.23.Cq, 71.15.Mb, 71.15.Pd

## I. INTRODUCTION

Amorphous silicon nitride (a-$Si_3N_{4-x}$:H) is commonly used in the solar cell industry because it has three desirable properties: It serves as antireflection coating and enhances light transmission, it is the main source of hydrogen (H) for passivating the silicon (Si) wafer, and it chemically and physically passivates the surface.[1] By changing deposition parameters, such as the gas flow of $NH_3$ and $SiH_4$, these properties of a-$Si_3N_{4-x}$:H can be easily varied and tuned to enhance solar cell efficiency.[2] The material is most commonly fabricated by plasma enhanced chemical vapor deposition (PECVD),[1,3,4] but other deposition methods like sputtering are used as well.[5,6]

Structural properties have been experimentally determined by Aiyama *et al.* and Misawa *et al.* using x-ray and neutron scattering.[7,8] Furthermore, trapping centers have been investigated by electroparamagnetic resonance (EPR) measurements by Lenahan *et al.* and Warren *et al.*[9,10] Experiments are mostly limited to mesoscopic and macroscopic investigations, which are difficult to link to structural and electronic properties at the atomic scale. In order to fill this gap, computer simulations are now commonplace to establish realistic atomic scale models and relate them to the observed macroscopic properties.

First insight into silicon nitrides at the atomic scale was provided by the seminal studies of Robertson *et al.* in the 1990s.[11–14] Robertson *et al.* applied tight-binding methods to small, essentially crystalline model systems and investigated defect induced changes in the electronic properties. These results are still helpful, but, with the advances in *ab initio* density functional theory, it is possible to study the properties of amorphous silicon nitrides in much greater detail and using better founded approximations.

In more recent computer simulations, typically a small selection of a-$Si_3N_{4-x}$:H configurations were produced in order to investigate the structural, electronic, and optical as well as vibrational properties.[15–26] Few of these studies examined even the materials properties for different stoichiometries[17,20,25] and the effect of hydrogenation.[18,21,22] Nevertheless, the number of considered models was generally very small making a statistically meaningful analysis difficult.

In order to build amorphous model structures, different strategies are adopted. A common strategy is to assemble small subunits and clusters with proper short-range order (SRO) into a continuous random network (CRN)[16] or Bethe lattice.[21,27] Furthermore, bond switching methods can be applied to the crystalline samples until they become reasonably amorphous.[22,28] Although very small defect concentrations are achievable by these strategies,[28] the most common and maybe most unbiased method to determine amorphous structures is by cooling the samples from the melt. This can be done by either Monte Carlo (MC)[17–19] or molecular dynamics (MD)[15,20,22–26,29] simulations.

As a matter of fact, all simulations need to rely on a potential-energy surface to calculate jump probabilities and forces during the cooling and relaxation. *Ab initio* methods are very desirable but incur great computational cost,[20,22–24,26] and hence many simulations are performed using different types of semiempirical potential models (e.g., Tersoff, tight binding, Keating, Busing, Born-Mayer-Huggins).[15–18,21,25,29] Both methods can also be combined in order to save computation time and/or to simulate larger systems. In this case, the samples are annealed using fast empirical potentials, and, afterwards, the electronic properties are calculated with more accurate *ab initio* methods.[19,29]

In the present work, we present large-scale periodic *ab initio* molecular dynamics studies on stoichiometric and nonstoichiometric $Si_3N_{4-x}$ including up to 10 at.% H. Typically, we prepare three carefully quenched reference configurations with about 200 atoms for each considered stoichiometry.

 ©2012 American Physical Society

To allow for a statistically meaningful evaluation of defect related properties, 1000 small structural models with 100 atoms are then prepared for each stoichiometry. The main focus of the present work is an evaluation of the small models against the larger models, as well an evaluation of the average structural properties such as the pair-correlation function, angular distribution function, structure factor, and general features of the electronic density of states as well as the average local coordination of the atoms. A detailed analysis of the defect related properties is presented in a separate publication.

## II. MODELING SETUP

### A. Compositions, concentrations, and densities

Nonstoichiometric amorphous silicon nitrides exhibit large density variations that seemingly depend strongly on the applied preparation conditions.[3,30,31]

Here we mainly focus on amorphous silicon nitrides as used in the solar cell industry and we decided to determine the densities from the data published by Ippolito and Meloni.[25] We found it helpful to plot the average experimental volume per atom versus the nitrogen concentration, as shown in Fig. 1. The volumes would lie on a straight line, if Vegard's law was observed.[33] Indeed, within the experimental uncertainties, this relation seems to hold very well, but the fit deviates from the volume of crystalline silicon in the Si rich case by more than 2%. Increasing the slope improves this behavior for the Si rich case (full line) without deteriorating the root-mean-square error for the amorphous samples significantly. The final densities and volumes, as obtained from the fitted experimental data, are summarized in Table I.

The second issue to address is the influence of hydrogen on the volume. The experimental data were almost always measured in the presence of substantial amounts of H approaching up to 25 at.%.[6] Remarkably, however, hydrogen seems to influence the volume only very little. For instance, although for the data shown in Fig. 1, the H content varies from 15 to 25 at.%, the deviation from Vegard's law is hardly noticeable, and for $Si_3N_4$ the volume of the amorphous structure agrees within a few percent with the volume of crystalline $\beta$-$Si_3N_4$. This observation is reinforced by considering the small covalent radius of hydrogen. Even if we double the covalent radius, $d_H = 2r_{covalent} = 0.62$ Å (this value corresponds to the H-H bond length), and determine the corresponding volume, $V_H = 4\pi d_H^3/3 \approx 1$ Å$^3$, we obtain only small corrections to the volume. If the concentration were 20 at.% H, it would take up at most 3% of the entire volume. This is certainly a rather crude consideration, since one could argue that hydrogen disrupts the usual bonding topology of the network and therefore might yield a significantly larger volume increase, but neither the experimental data nor any of our results seem to support this idea. Most likely, hydrogen simply accommodates in the network at defective or highly strained sites and hence causes only negligible changes in the volume.

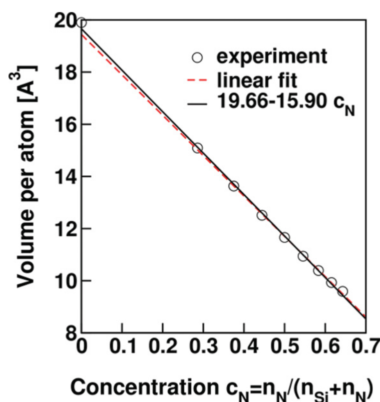


FIG. 1. (Color online) Volume per atom as a function of the N concentration $c_N = n_N/(n_N + n_{Si})$. The broken line shows the best linear fit to the experimental values (circles). The full line was obtained by readjusting the fit such that the density of crystalline Si is more accurately reproduced. This has only a slight effect on the root-mean-square error. The experimental data points for $Si_3N_x$:H are from Guraya *et al.* (Ref. 6) the density for crystalline Si is from Ashcroft and Mermin (Ref. 32).

TABLE I. Densities $\rho$ and volumes per atom of $Si_3N_x$ as studied in the present work. The densities were derived from experimental values as shown in Fig. 1 (see also Guraya *et al.*) (Ref. 6). The table also shows the supercell volumes and the number of silicon $n_{Si}$ and nitrogen atoms $n_N$ in the considered supercells.

| | $Si_3N_{4.5}$ | $Si_3N_4$ | $Si_3N_{3.5}$ | $Si_3N_3$ |
|---|---|---|---|---|
| $\rho$ (g/cm$^3$) | 3.22 | 3.14 | 3.06 | 2.98 |
| Volume per atom (Å$^3$) | 10.12 | 10.57 | 11.10 | 11.71 |
| $n_N/(n_{Si}+n_N)$ | 0.60 | 0.57 | 0.54 | 0.50 |
| Large supercell vol. (Å$^3$) | 1973 | 1999 | 2020 | 2014 |
| $n_{Si}$ | 78 | 81 | 84 | 86 |
| $n_N$ | 117 | 108 | 98 | 86 |
| Small supercell vol. (Å$^3$) | 1012 | 1033 | 1020 | 1077 |
| $n_{Si}$ | 40 | 42 | 42 | 46 |
| $n_N$ | 60 | 55 | 50 | 46 |

To determine the hydrogen concentration typically found in a-$Si_3N_{4-x}$:H layers used in the fabrication of industrial solar cells, over 80 different $Si_3N_{4-x}$:H samples were prepared with plasma enhanced chemical vapor deposition (PECVD) at the Energy Research Center of the Netherlands. A more detailed description of the PECVD method is given by Soppe.[2] The samples were analyzed using Fourier transform infrared spectroscopy (FTIR) and ellipsometry. From these data, the atomic concentration was extracted using the approach described by Bustarret *et al.* (see Fig. 2).[34] We expect that the hydrogen concentration is rather low for the stoichiometric case and, although the data show a large scatter towards the right side of the graph ($Si_3N_4$), and the hydrogen concentration increases again for over-stoichiometric samples ($Si_3N_{4+x}$), we decided to perform the simulations for the $Si_3N_4$ case without hydrogen. For the other, nitrogen deficient cases, we performed simulations without hydrogen and with approximately 13 at.% H. This seems to be well within the experimental range, which lies between 10 and 15 at.% H for the considered stoichiometries.

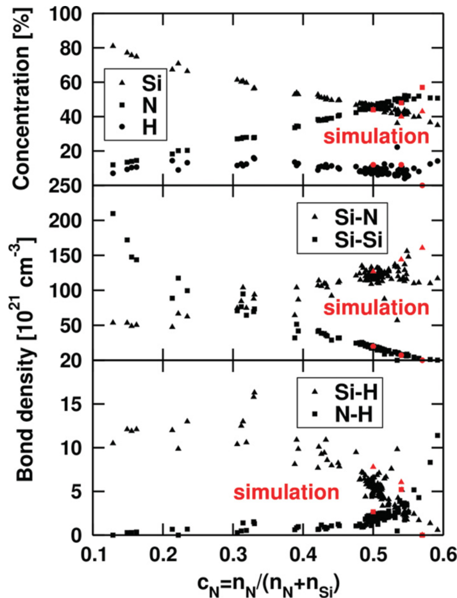


FIG. 2. (Color online) Atomic concentration and bond densities estimated for plasma-enhanced-chemical-vapor depositioned (PECVD) silicon nitride. The dependency of the nitrogen concentration $c_N$ is shown. The stochiometric case ($Si_3N_4$) is to the right. The values obtained by simulations are marked with red symbols at $c_N = 0.50$, 0.54, and 0.57 for $Si_3N_3H_{0.8}$, $Si_3N_{3.5}H_{0.8}$, and $Si_3N_4$, respectively.

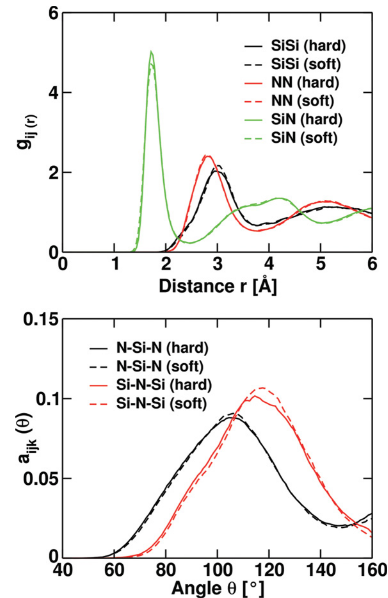


FIG. 3. (Color online) The PC functions $g_{ij}(r)$ and angular distribution functions $a_{ijk}(\Theta)$ of a-$Si_3N_{3.5}$ at 3000 K for different potentials. The soft potential (150 eV) used in our calculations gives within statistical uncertainties the same results as the harder reference (300 eV).

### B. PAW potentials and technical parameters

All calculations presented in this work were performed using the Vienna *ab initio* simulation package (VASP) and projector augmented wave (PAW) potentials in the implementation of Kresse and Joubert.[35–38] VASP uses periodic (or cyclic) boundary conditions, a Brillouin-zone sampling at the Γ point, and the PBEsol functional (Perdew-Burke-Ernzerhof functional revised for solids).[39]

Since our aim was to perform large scale simulations, we decided to construct special PAW potentials optimized for the specific application in mind. To this end, we chose for the PAW potentials the largest possible core radius that did not degrade the quality of the results noticeably. We found that core radii of 2.0 and 1.9 a.u. (2.5 and 2.4 a.u.) for the *s*-partial (*p*-partial) waves for N and Si, respectively, lead to acceptable results. For Si the *d* potential was chosen as local potential, whereas for N the all-electron potential was smoothed inside a sphere with a radius of 0.8 a.u. These potentials allowed us to obtain converged total energies at a plane-wave kinetic energy cutoff of about 150 eV. Results for bulk Si are essentially indistinguishable from more accurate PAW potentials, whereas results for $Si_3N_4$ are slightly deteriorated compared to accurate reference calculations, but the errors remain fairly small. The $Si_3N_4$ volumina of the bulk crystalline phases ($\alpha$, $\beta$, and $\gamma$) are reproduced to within 1.5%, and the relative energy difference between the $\alpha$ and $\gamma$ phase, which is 1.05 eV per formula unit using accurate reference potentials, is reproduced to within 0.03 eV. The largest errors are observed for the zone centered phonons where discrepancies of the order of 5.0% for some high-frequency branches are observed, whereas the predicted DFT Kohn-Sham band gaps agree within 2% with the accurate reference potential. In summary, the differences between the accurate reference potentials and the soft potentials are of the same order as the differences between the local-density approximation and gradient corrected density functionals, which we believe to be a reasonable threshold. Furthermore, for liquid $Si_3N_{3.5}$ only small differences were found for the pair-correlation (PC) function and angular distribution function at 3000 K (see Fig. 3). For over-stoichiometric samples, however, the N-N distance is shifted by 0.2 Å to larger bond distances using the soft potentials, but this will not change the results for the experimentally relevant under-stoichiometric samples. This makes us confident that the present PAW potentials give accurate results and are certainly far superior to conventional molecular dynamics potentials such as the Tersoff potential.[25] Compared to the standard potentials requiring 400 eV cutoff, the savings are about a factor 5, and they allow us to perform much longer simulations than otherwise possible.

#### *1. Large simulation cells, slow annealing*

Our initial strategy was to determine representative samples by cooling from the melt using fairly large simulation cells with a total supercell volume of about 2000 Å$^3$. Table I summarizes the corresponding supercell volumes and the number of atoms we employed.

All systems were initially molten at 4000 K and then the temperature was gradually decreased until the atomic configuration started to freeze in. In all simulations, a time step of 1.5 fs was adopted, and the mass of hydrogen was increased to 10 amu. This mass increase will change the dynamics of the system, but has no influence on the explored configuration space as the partition function factorizes into a momentum

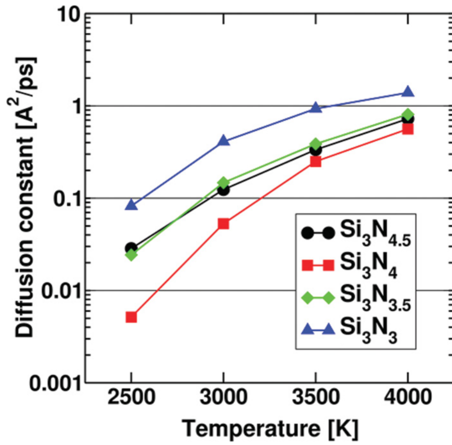


FIG. 4. (Color online) Diffusion constants for $Si_3N_x$ averaged over both atom types at different temperatures. Stoichiometric $Si_3N_4$ (red squares) always shows the highest freezing temperature.

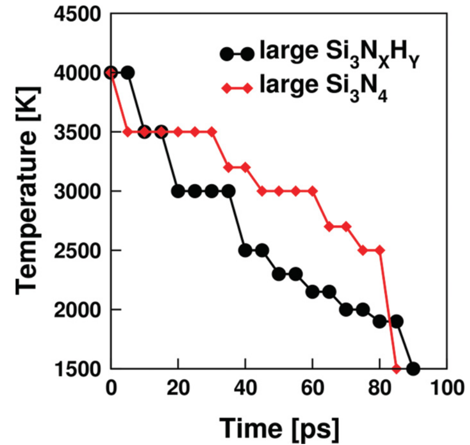


FIG. 5. (Color online) Annealing history adopted in the present work for the large $Si_3N_x$ systems. Because $Si_3N_4$ freezes at about 3100 K, the system was equilibrated for 30 ps at 3500 K, then the system was cooled to 3000 K and annealed at this temperature until most defects were removed. For the other stoichiometries, 20 ps annealing was performed at 3000 K, and then the temperature was gradually decreased to 2000 K equilibrating at each temperature for 10 ps.

and configuration dependent part, with the latter one being independent of the masses.

The "freezing" temperature was strongly dependent on the stoichiometry, as demonstrated in Fig. 4, where the diffusion constant averaged over both atom types is plotted versus the temperature. When the value drops significantly below 0.05–0.1 $Å^2$/ps, it is difficult to determine accurate diffusion constants. Monitoring the mean-square displacement for these cases indicates jump diffusion occurring every few ps. It is likely that this is defect mediated, since the network can easily re-adjust and re-link at defects, and, consequently, the defect might migrate through the network. But a detailed investigation of this issue is beyond the scope of the present work. Stoichiometric $Si_3N_4$ freezes in at about 3000–3100 K on a time scale of 20–40 ps, which we observed repeatedly for several simulations at different system sizes, and the freezing goes along with the geometrical defects being progressively removed during the annealing. Usually the system locks in when two or zero defects are present in the sample (for topological reasons the defects always come in pairs for stoichiometric $Si_3N_4$). The observed amorphization temperature seems to be significantly larger than the experimental estimates of about 2000 K.[40,41] But we note that the melting temperature of silicon nitride cannot be measured, since the solid decomposes into atomic and molecular Si and N before melting sets in (gas pressure of Si).

Matter of fact, our simulations are also hampered because of the short time scales and small system sizes that are accessible to us: once all defects are cured, the system freezes. In real experimental samples, the density of mobile defects will only exponentially approach zero, sustaining diffusion at much lower temperatures. Furthermore, we believe that the experimental samples are never perfectly stoichiometric. Even being slightly off-stoichiometric, diffusion is enhanced since some defective bonds (e.g., Si-Si bonds) or coordination defects prevail. For $Si_3N_{3.5}$ and $Si_3N_{4.5}$, amorphization occurs at roughly 2600 K, whereas, for $Si_3N_3$, the freezing occurs at roughly 2300 K. We also note that jump diffusion is well possible below these temperatures, but these events are very rare on the time scales accessible to us. Finally, addition of 10 at.% H generally lowers the amorphization temperature by another 200 K (not shown).

The adopted temperature profiles are shown in Fig. 5. In retrospect, we could have fine tuned the cooling history somewhat for each stoichiometry, for instance by progressively elongating the runs when approaching the freezing temperature, but we believe that this will change the final results only little. In order to prepare a set of samples, we extended the simulation runs at 3500 K ($Si_3N_4$) and 3000 K ($Si_3N_{4-x}$:H) followed by the same annealing history as for the original samples. In this manner, three samples were generated for each of a-$Si_3N_4$, a-$Si_3N_3$, a-$Si_3N_{3.5}$. For the less relevant a-$Si_3N_{4.5}$ and the hydrogenated samples only a single large representative structure was generated.

#### 2. *Small simulation cells*

The drawback of the strategy adopted above is that it is difficult to generate any statistics for the defect related properties. Even with three samples, we cannot determine how likely the formation of a certain defect class is. To complement the simulations of the large systems, we therefore performed simulations for smaller systems containing about 100 atoms. In this case, the simulation was run for up to 1 ns just above the freezing temperature, and every 500–1000 steps a configuration was quenched into the closest local energy minimum using a standard minimization procedure. This approach allowed us to generate about 1000 reasonably independent samples for each stoichiometry. The corresponding runs typically required 4 weeks on 32 cores each.

In Fig. 6, we show the acquired mean-square displacements (MSDs) for four different stoichiometries. The diffusion constants are roughly similar and constant over the simulation time. Lowering the temperature by 50–100 K usually resulted in rapid freezing of the structures. The chosen stoichiometries correspond roughly to the same stoichiometries as those

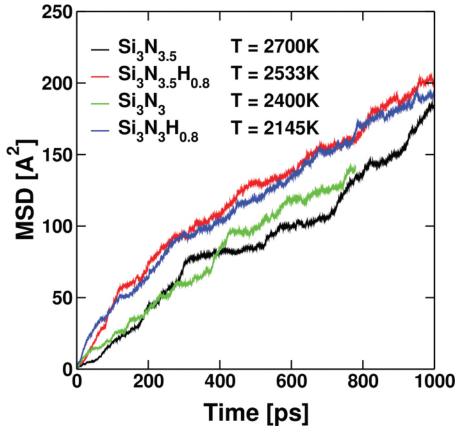


FIG. 6. (Color online) Mean-square displacements (MSDs) for four different $Si_3N_{4-x}$:H ensembles. The averaged temperature is given after the system label. The temperatures were adjusted to keep the ensembles just above the freezing temperature. In some cases, the temperature had to be increased and the simulation restarted before the freezing, when accidental freezing occurred.

considered for the large systems. Only for the "stoichiometric" case, we removed one N atom resulting in a stoichiometry of roughly $Si_3N_{3.9}$ in order to avoid that all defects accidentally annihilate, which might have resulted in a "lock-in" at temperatures even above 3100 K.

## III. STRUCTURAL PROPERTIES

The main focus of the present work is on general structural properties, whereas a detailed analysis of the electronic properties of defects and defect statistics is reserved for a later publication. In the following sections we evaluated the pair-correlation function, structure factor, angular distribution function, and the local bonding topology at the Si and N sites.

### A. Pair-correlation function

The pair-correlation (PC) functions for the quenched amorphous samples are shown in Fig. 7. For the large systems, the results were averaged over three samples (except for $Si_3N_{4.5}$, where only a single structure was generated), whereas for the small systems the average was done over about 1000 samples. In addition to the PC function, we analyzed the average number of nearest neighbors by integration of the partial PC functions between 0 and the first minimum $r_{\min}$ in the respective function (see Table II):

$$N_{ij} = \rho_{h_j} \int_0^{r_{\min}} dr 4\pi r^2 g_{ij}(r). \tag{1}$$

Also the mean bonding distance $\bar{d}_{ij}$ and the standard deviation $\sigma_{ij}$ were evaluated by integrating up to the first minimum (see Table III).

The first important observation is that the PC functions of the small (black solid lines) and the large systems (black broken lines) are very similar, in particular, at large distances beyond the first nearest neighbor. This is a little

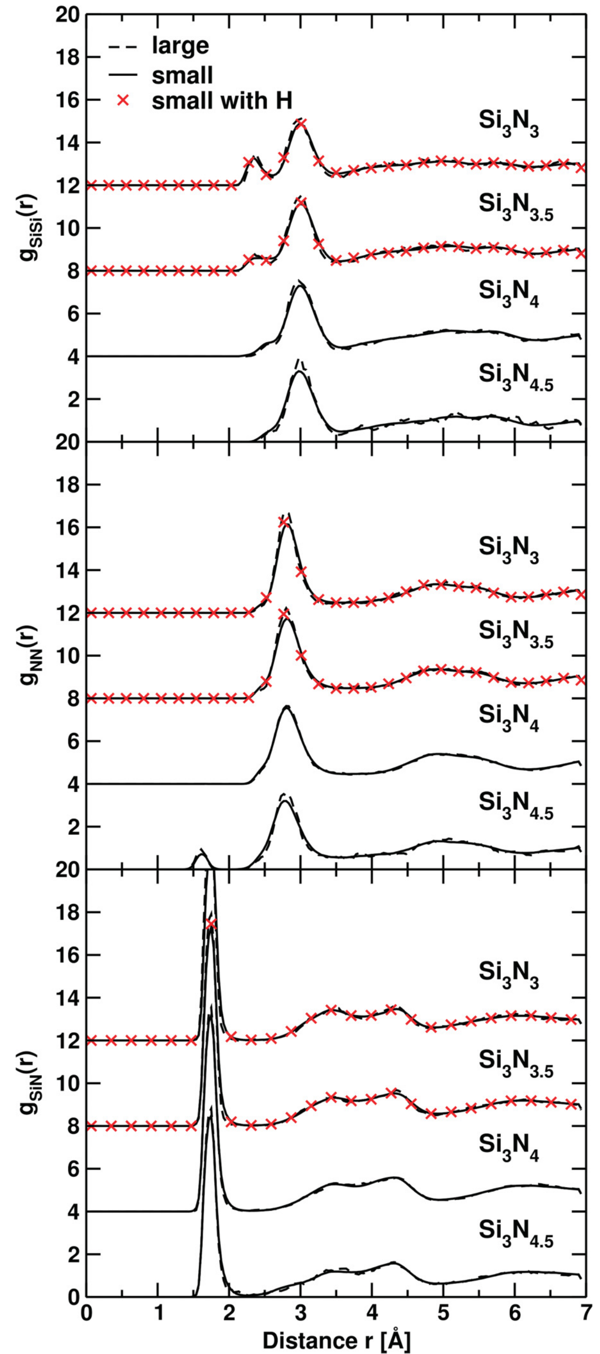


FIG. 7. (Color online) Partial pair-correlation functions $g_{ij}(r)$ for the small (full line) and the large $Si_3N_x$:H systems (broken line). Hydrogen (crosses) leaves the PC function largely unchanged.

bit counterintuitive since we can rather expect differences at long distances due to finite-size effects, but at large distances we only recognize slightly more scatter for the large systems, which points towards insufficient sampling over different configurations. However, at the distance of the first nearest neighbor, the PC function for the large systems shows somewhat more pronounced and narrower peaks for N-N and Si-Si. We believe that this is related to the slower and more careful annealing performed for the large systems. Recall that the small systems were created by directly

TABLE II. The partial coordination numbers $N_{ij}$ evaluated for small ensembles. $N_{ij}$ specifies for atom $i$ the number of nearest neighbors of type $j$.

| | $Si_3N_{4.5}$ | $Si_3N_4$ | $Si_3N_{3.5}$ | $Si_3N_3$ |
|---|---|---|---|---|
| $N_{SiN}$ | 4.16 | 3.95 | 3.57 | 2.99 |
| $N_{SiSi}$ | | | 0.38 | 1.01 |
| $N_{NSi}$ | 2.77 | 3.02 | 3.00 | 2.99 |
| $N_{NN}$ | 0.30 | | | |
| | $Si_3N_{3.5}H_{0.4}$ | $Si_3N_{3.5}H_{0.8}$ | $Si_3N_{3.5}H_{1.7}$ | $Si_3N_3H_{0.8}$ |
| $N_{SiN}$ | 3.51 | 3.47 | 3.40 | 2.97 |
| $N_{SiSi}$ | 0.48 | 0.35 | 0.33 | 0.93 |
| $N_{NSi}$ | 2.94 | 2.91 | 2.85 | 2.97 |
| $N_{NN}$ | | | | |
| $N_{HSi}$ | 0.51 | 0.51 | 0.47 | 0.70 |
| $N_{HN}$ | 0.48 | 0.44 | 0.38 | 0.24 |
| $N_{HH}$ | 0.04 | 0.06 | 0.13 | 0.06 |

quenching from the melt. In all other respects, the small systems seem to adequately represent the amorphous structure, and specifically finite-size effects at large distances are largely absent in the small simulation cell, at least at the level of the PC function.

The second remarkable observation is that hydrogen, in the low concentrations considered here, has virtually no discernible effect on the PC function (compare full line with red crosses). It rather seems that hydrogen only participates as a "spectator" decreasing the connectivity and increasing self-diffusion, with no dramatic effect on the *average* structural properties of the amorphous structure, as evaluated by the PC

TABLE III. Mean bonding distances and standard deviations and position of the minimum in the pair-correlation function of the $Si_3N_x$ evaluated for small ensembles (all values are in Å). For the nonstoichiometric systems, peaks emerge at short distance corresponding to direct Si-Si and direct N-N neighbor atoms at 2.4 and 1.6 Å, respectively.

| Si-Si | $Si_3N_{4.5}$ | $Si_3N_4$ | $Si_3N_{3.5}$ | $Si_3N_3$ |
|---|---|---|---|---|
| 1st $\bar{d}_{SiSi}$ | | | 2.40 | 2.38 |
| 1st $\sigma_{SiSi}$ | | | 0.10 | 0.10 |
| 1st $r_{min}$ | | | 2.57 | 2.59 |
| 2nd $\bar{d}_{SiSi}$ | 3.00 | 2.99 | 3.02 | 3.02 |
| 2nd $\sigma_{SiSi}$ | 0.22 | 0.24 | 0.19 | 0.19 |
| 2nd $r_{min}$ | 3.56 | 3.56 | 3.53 | 3.49 |
| N-N | $Si_3N_{4.5}$ | $Si_3N_4$ | $Si_3N_{3.5}$ | $Si_3N_3$ |
| 1st $\bar{d}_{NN}$ | 1.62 | | | |
| 1st $\sigma_{NN}$ | 0.06 | | | |
| 1st $r_{min}$ | 1.98 | | | |
| 2nd $\bar{d}_{NN}$ | 2.86 | 2.89 | 2.90 | 2.89 |
| 2nd $\sigma_{NN}$ | 0.26 | 0.26 | 0.25 | 0.23 |
| 2nd $r_{min}$ | 3.54 | 3.62 | 3.63 | 3.58 |
| Si-N | $Si_3N_{4.5}$ | $Si_3N_4$ | $Si_3N_{3.5}$ | $Si_3N_3$ |
| 1st $\bar{d}_{SiN}$ | 1.75 | 1.75 | 1.75 | 1.75 |
| 1st $\sigma_{SiN}$ | 0.09 | 0.08 | 0.07 | 0.07 |
| 1st $r_{min}$ | 2.26 | 2.30 | 2.30 | 2.30 |

function. For $Si_3N_{3.5}H_{0.8}$ and $Si_3N_3H_{0.8}$, the mean hydrogen bonding distances are $0.77 \pm 0.01$ Å for $\bar{d}_{HH}$, $1.50 \pm 0.07$ Å for $\bar{d}_{HSi}$, and $1.11 \pm 0.04$ Å for $\bar{d}_{HN}$.

The present PC functions agree very well with previous simulations. The Si-N PC functions shows a pronounced peak at 1.75 Å, which hardly shifts with varying stoichiometry, and in fact, the entire Si-N PC function is almost independent of stoichiometry. Inspection of Table II shows that each N atom forms three bonds, whereas the number of bonds formed by the Si atoms is always very close to 4 (the sum of $N_{SiN}$ and $N_{SiSi}$). For stoichiometric $Si_3N_4$, the Si-Si PC function shows one strong peak at 3.0 Å, which is related to the distance between Si atoms in Si-N-Si triangles, and similarly the N-N PC function shows a peak at 2.90 Å related to N-Si-N triangles. The other feature worth mentioning is the small shoulder in the Si-Si PC function around 2.6 Å. As already discussed by Giacomazzi *et al.*, it is mostly related to planar Si-N-Si-N squares.[23] For substoichiometric $Si_3N_{4-x}$, this peak seems to develop into a pronounced shoulder around 2.4 Å, but in fact, the origin of this shoulder is direct Si-Si bonds, as shown in the number of direct Si-Si neighbors $N_{SiSi}$ in Table II, which increases from 0.38 in $Si_3N_{3.5}$ to 1 in $Si_3N_3$. Likewise, direct N-N bonds form in over stoichiometric $Si_3N_{4+x}$, as indicated by a value of $N_{NN} = 0.3$ in $Si_3N_{4.5}$. The absence of direct N-N neighbors in stoichiometric and substoichiometric $Si_3N_{4-x}$, and likewise the absence of direct Si-Si neighbors in stoichiometric and over-stoichiometric $Si_3N_{4+x}$ is a clear indication for the strong ordering tendency in silicon nitrides, as direct bonds to the same species are only formed if the material contains too much Si (Si-Si bonds) or too much N (N-N bonds). In summary, the amorphous structures are characterized by (i) fourfold coordinated Si atoms and threefold coordinated N atoms, with (ii) a strong tendency towards heterocoordination and formation of Si-N bonds. The partial coordination numbers also reveal that hydrogen indeed disrupts the normal network topology of silicon nitride. For $Si_3N_{3.5}H_{0.8}$, it forms bonds with both Si and N atoms, whereas for $Si_3N_3H_{0.8}$ bonds are predominantly formed to Si atoms. Of course such bonds reduce the number N-Si bonds, for instance $N_{NSi}$ drops from 3.0 to 2.91 in $Si_3N_{3.5}H_{0.8}$, and the sum $N_{SiSi} + N_{SiN}$ decreases from 4 to 3.9 when hydrogen is added in $Si_3N_3H_{0.8}$.

To investigate the dependence on the H content, we also performed calculations for concentrations of 6 and 20 at.% H for $Si_3N_{3.5}$. As can be recognized from Table II, the probability that hydrogen attaches to silicon or nitrogen is pretty much independent of the H content, but changes with stoichiometry. For $Si_3N_{3.5}$ and $Si_3N_3$, about 50% and 70% of the H bonds to Si, respectively, whereas the number of hydrogen bonded to nitrogen decreases with decreasing N content. These results are in good agreement with experiments (compare Fig. 2 bottom panel; also see Refs. 6 and 42). It is also quite clear and not unexpected that the number of H "dimers" increases with the H content, but it remains fairly small up to about 10–15 at.% H.

For stoichiometric $Si_3N_4$, we can compare the present bonding distances and the bonding angles with experimental data obtained by Aiyama *et al.* and Misawa *et al.*[7,8] and with results from the simulations performed by Giacomazzi *et al.* and Jarolimek *et al.*[23,24] The present mean values have been calculated by averaging the bond length over the bonds up

TABLE IV. Reference values for the bond lengths in a-$Si_3N_4$ obtained by experiments and simulations (all values are in Å).

| Ref. | 1st $\bar{d}_{SiSi}$ | 2nd $\bar{d}_{SiSi}$ | 2nd $\bar{d}_{NN}$ | 2nd $\bar{d}_{SiN}$ |
|---|---|---|---|---|
| Aiyama *et al.* (Ref. 7) | | 3.00 | 3.00 | 1.75 |
| Misawa *et al.* (Ref. 8) | | 3.01 | 2.83 | 1.73 |
| Giacomazzi *et al.* (Ref. 23) | 2.42 | 3.03 | 2.76 | 1.73 |
| Jarolimek *et al.* (Ref. 43) | 2.35–2.41 | 3.10 | 2.90 | 1.76 |

to the first minimum $r_{min}$ tabulated in Table III. Our mean distances are 3.0 Å for $\bar{d}_{SiSi}$, 2.9 Å for $\bar{d}_{NN}$, and 1.75 Å for $\bar{d}_{SiN}$. These values agree very well with previous experiments and simulations, as shown in Table IV.

For Si rich samples, the direct Si bond distance is located at 2.4 Å, again in excellent agreement with previous simulations for amorphous $Si_3N_x$:H (and in good agreement with simulations for amorphous Si).[23,24,43]

Over-stoichiometric $Si_3N_{4.5}$ was investigated by Ippolito and Meloni using Tersoff potentials finding a peak in the N-N PC function around 1.3 Å.[25] In view of our present value of 1.62 Å this seems a little bit too short, but we have already emphasized that this peak distance is somewhat overestimated due to the use of a very soft N potential. After relaxation using harder potentials, the mean distance moves to 1.45 Å, which is still larger than the value for the Tersoff potential. Our present simulations also agree with previous *ab initio* simulations in predicting no direct N-N neighbors in stoichiometric and substoichiometric $Si_3N_{4-x}$, whereas the previous force field simulations showed direct N-N bonds even in slightly substoichiometric $Si_3N_{4-x}$. This clearly points towards some deficiency in the Tersoff force fields.

### B. Angular distribution function

In Fig. 8, we show the angular distribution functions for different $Si_3N_x$ compositions, with and without hydrogen. As before for the pair-correlation function, hydrogen influences the angular distribution function very little, and results for the large and small system (without hydrogen) are very similar. Regardless of stoichiometry, the main peaks are located at mean angles of 110° for silicon, and 120° for nitrogen. The value of $120° = 360°/3$ is in perfect agreement with the value expected for a flat triangle formed by three Si atoms surrounding a central N atom. This again confirms that the local bonding topology of nitrogen changes very little compared to crystalline $Si_3N_4$, where each N atom is surrounded by three Si atoms forming a coplanar triangle. This is also consistent with the electronic configuration of nitrogen, forming three $sp^2$ hybrid orbitals that interact with the three Si neighbors, and one out-of-plane lone pair $p$ orbital that is doubly occupied and oriented perpendicular to the $NSi_3$ plane. Furthermore, a second peak is visible at 90° in the angular distribution function. This peak stems from N-N neighbors in a planar Si-N-Si-N arrangement, as shown in the inset.

The bond angle distribution for silicon is strongly peaked at a mean angle of 110° agreeing perfectly with the expected tetrahedral bonding angle of 109.5°. As for nitrogen, this suggests that the Si atoms maintain their $sp^3$ hybridization

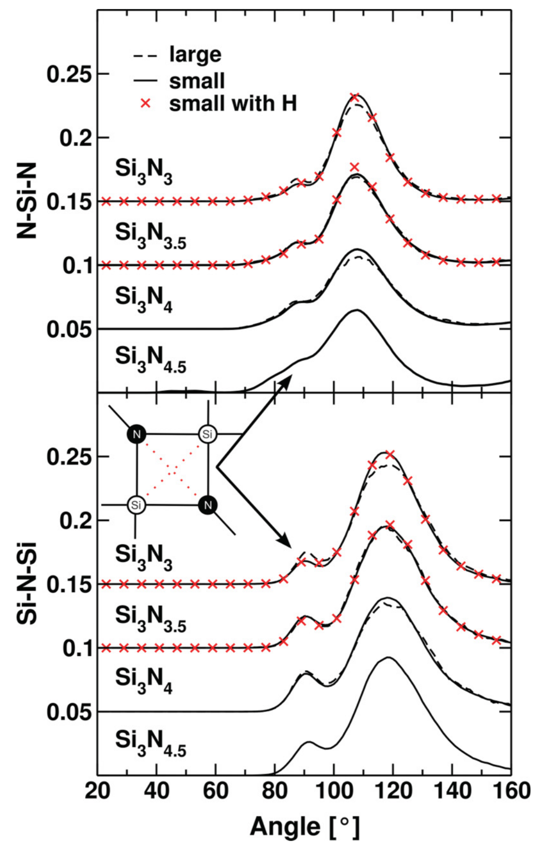


FIG. 8. (Color online) The angular distribution functions of $\measuredangle_{SiNSi}$ and $\measuredangle_{NSiN}$ for the large and the small $Si_3N_x$:H systems relative to the same distribution in a hypothetical ideal gas with the same density and composition. The distribution function is, therefore, normalized by a factor of $1/\sin(\theta)$ amplifying contributions at 0° and 180°. Two Si and two N atoms arranged in a square result in pronounced peaks at 90°.

forming bonds with the four neighboring atoms. These are N atoms in the stoichiometric case, and possibly few Si atoms in the substoichiometric case $Si_3N_{4-x}$. Again a clear secondary peak is visible at 90° related to the planar Si-N-Si-N arrangement already mentioned above. For both silicon and nitrogen this peak loses intensity when moving to substoichiometric compositions. This relates well to the observation that the number of Si-N-Si-N square configurations decreases when the amount of nitrogen deviates from the perfect stoichiometry $Si_3N_4$.

Finally, comparison of the large and small systems shows that the $Si_3N_3$ angular distribution function is slightly overstructured for the small simulation cells. We believe that this is related to finite-size effects and the artificial periodicity. The introduced errors are, however, small and seem to have negligible effects on other properties such as the electronic density of states.

### C. Structure factor

Information about long-range order and density fluctuations are most easily investigated by an ensemble average of the

Faber-Ziman structure factor $S(\mathbf{k})$,[44–47]

$$S(\mathbf{k}) = \frac{1}{N}\left\langle \sum_i \sum_j \exp[-i\mathbf{k}(\mathbf{r}_i - \mathbf{r}_j)] \right\rangle, \qquad (2)$$

where $\mathbf{k}$ are wave vectors and $N$ is the total number of atoms and $\mathbf{r}_i$ are the atomic positions. Consistent with the finite supercell, we evaluated the structure factor on a grid of reciprocal-lattice vectors $\mathbf{k}$ that are compatible with the applied supercell (and not by a Fourier transformation of the pair-correlation function). From the structure factors $S(\mathbf{k})$ on the grid, the isotropic structure factor is calculated by averaging over different $\mathbf{k}$ orientations and properly weighing each contribution:

$$S(q) = \frac{\int S(\mathbf{k})\,\delta(|\mathbf{k}| - q)\,d^3k}{4\pi q^2}. \qquad (3)$$

The partial structure factors for each atom type $S_{\alpha\alpha}(q)$ were obtained by summation over one atom type in Eq. (2), and the partial structure factor $S_{\alpha\beta}(q)$ with $\alpha \neq \beta$ was determined by

$$S_{\alpha+\beta}(q) = \sum_{\alpha\beta} (c_\alpha c_\beta)^{1/2} S_{\alpha\beta}(q), \qquad (4)$$

where $c_\alpha$ is the concentration of atom type $\alpha$ and $S_{\alpha+\beta}(q)$ is the total structure factor of both atom types.[46]

In Fig. 9 the structure factors are shown for the large supercells, since the small simulation cells result in a fairly coarse reciprocal-space grid, causing a jagged behavior (qualitatively the results are, however, similar as one would expect from the close agreement for the pair-correlation function).

In general, the structure factors change little with composition, and in all cases, the main peak is observed at 2.2 $Å^{-1}$ which agrees with the results of Jarolimek *et al.*[24] The corresponding wavelength is roughly 2.8 Å agreeing well with the typical Si-Si and N-N distances in the pair-correlation function. This indicates that the peak is mostly a residual of the Fourier transform of the first peak in the pair correlation, rather than a true long-range order. Remarkably, the SiN structure factor shows a strong anticorrelation at this wavelength, indicating a moderate medium-range order with alternating Si-N-Si-N planes where the distance between the Si-Si and N-N planes is roughly 2.8 Å. This medium-range order clearly decreases when moving off stoichiometry, most likely because Si-Si bonds are introduced into the network necessarily causing a disruption of the alternating planes.

The other important observation is the increase of the NN structure factor $S_{NN}$ at small wave vectors $\mathbf{q}$ with decreasing Si content. A similar increase is also observed for the small samples (not shown). Such an increase usually indicates the onset of long-range density fluctuations, i.e., there are regions in the simulation cell where N accumulates and regions where N becomes depleted. For sufficiently large simulation cells and sufficiently long simulation times, one might observe phase separation into a Si rich part with few N impurities, and a close-to-stoichiometric $Si_3N_4$. However, for the simulation cells and stoichiometries considered here, this effect was hardly noticeable in real space. As shown in the next section,

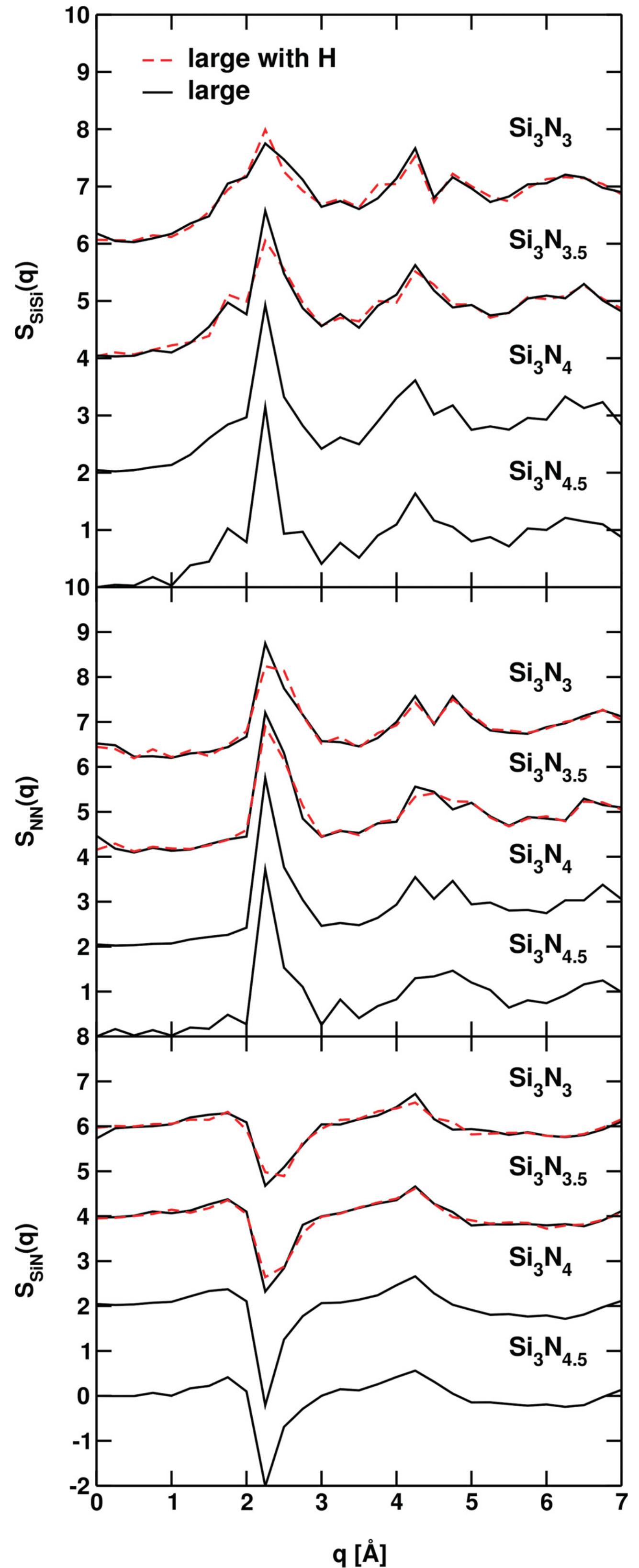


FIG. 9. (Color online) Partial Faber-Ziman structure factors $S_{\alpha\beta}(q)$ for the large $Si_3N_x$:H systems.

some residual of the phase separation is observable even in the local coordination upon careful investigation.

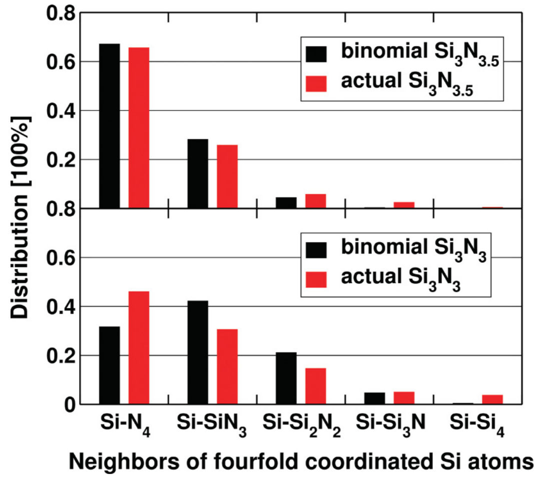


FIG. 10. (Color online) Detailed analysis of the bonding topology for fourfold coordinated Si atoms. The actual probability of finding a Si atom coordinated to $n$ N and $(4-n)$ Si atoms is shown. Also shown is the distribution that one would expect if the formation of a Si-Si bond were entirely random. Excess probabilities are found towards the two end points, in particular for $Si_3N_3$, which is consistent with a tendency towards Si clustering and "phase separation."

### D. Clustering or simple percolation

We now briefly return to the analysis of the local bonding properties of Si. As we have already shown in Table II, most Si atoms have four nearest neighbors, whereas the N atoms are all threefold coordinated. Furthermore Table II shows that N atoms form bonds exclusively to Si in the stoichiometric and substoichiometric case $Si_3N_{4-x}$ ($N_{NSi}$). In the absence of H, this allows us to estimate the partial Si coordination number to be $N_{SiSi} = x$, which is indeed roughly observed in Table II.

If the formation of Si-Si bonds were random, we would expect that the distribution of fourfold coordinated Si atoms with $n$ nitrogen and $(4-n)$ silicon neighbors would be roughly binomial,

$$p(n) = \frac{4!}{n!(4-n)!}\left(\frac{x}{4}\right)^{(4-n)}\left(\frac{4-x}{4}\right)^{n}. \qquad (5)$$

In Fig. 10 we show the actual distribution of the bonding topology of fourfold coordinated Si atoms and compare it with the binomial distribution. The most notable observation is that, while we would not expect any Si atoms with three Si neighbors in $Si_3N_{3.5}$ and any Si atoms with four Si neighbors in $Si_3N_3$, the actual analysis shows that such atoms exist. This is a sign that Si prefers either exclusively N neighbors or exclusively Si neighbors, which is consistent with our previous analysis of the structure factor and supports the claim that a tendency towards phase separation exists, although in the present case, it manifests itself only in the form of a slight tendency towards Si clustering, which goes beyond what one would expect for a random percolating network.

## IV. ELECTRONIC PROPERTIES

### A. Density of states

The silicon and nitrogen projected electronic density of states (DOS) is provided in Fig. 11, together with the DOS of crystalline $\beta$-$Si_3N_4$, which was already discussed by Kresse *et al.*[48] Averaging was done over all small samples (approximately 1000 for each stoichiometry). To align the individual DOS for different configurations and stoichiometries, we have chosen the average nitrogen 1$s$ core-level energies as reference.

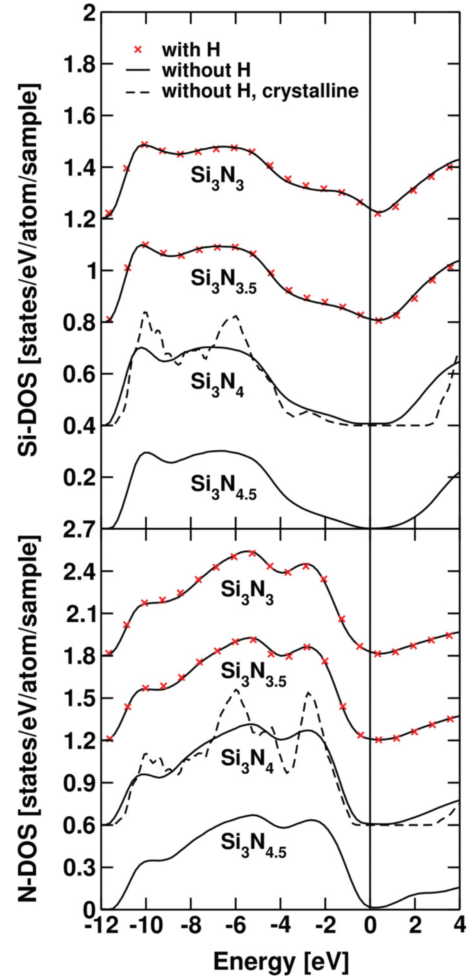


FIG. 11. (Color online) Site projected electronic DOS for Si and N atoms in the small $Si_3N_x$:H systems. The broken line corresponds to the DOS of crystalline $\beta$-$Si_3N_4$. The density of states are aligned in a such a way that the N core levels have always the same energy. The Fermi levels are located exactly at the minimum of the individual DOS.

Since the local short-range order of a-$Si_3N_4$ is very similar to $\beta$-$Si_3N_4$, we expect similar electronic properties as in the crystalline phases, which is indeed confirmed (compare with the broken line in Fig. 11). As for structural properties, we again find that hydrogen has virtually no discernible influence on the average electronic properties, although a detailed discussion of the properties of the defect states close to the Fermi level is postponed to a later study.

The lowest valence band is made up by N 2$s$ states (not shown). The second lowest subband ($-11$ to $-4$ eV) is predominantly made up by bonding N 2$p$ states. As already discussed, N atoms are located in an almost planar triangular configuration with 3 Si neighbors ($NSi_3$). The N 2$p$ band is

made up by two $p$ orbitals per N atom, and shows significant hybridization with Si $p$ states in particular at energies around $-10$ eV. The final subband below the Fermi level at $-2.5$ eV is dominated by the nonbonding N $2p$ states (one orbital per N atom) that is oriented out of the plane formed by the $NSi_3$ triangle. This band shows only very little hybridization with Si. As the Si concentration increases, a marked change is observed in the DOS below the Fermi level with a significant increase in the Si DOS and little to no changes in the N DOS. In stoichiometric $Si_3N_4$, the dominant contribution to the electronic states below the Fermi level is originally from the N $2p$ lone pair orbitals, however, for $Si_3N_{4-x}$ the Si DOS just below the Fermi level increases rapidly with decreasing N content. This property is easily understood to result from the increase in the number of Si-Si bonds. The bonding antiboding splitting for a Si-Si bond is far smaller than for the shorter Si-N bond: for a Si-N bond, the bonding Si-$3p$ N-$2p$ linear combination is pushed at least $-3$ eV below the Fermi level, whereas for a Si-Si bond, the bonding linear combinations is located just below the Fermi level. As a matter of fact, this also relates to the smaller band gap in crystalline Si or amorphous Si (compared to $Si_3N_4$). We thus expect that valence-band defect states have important contributions from Si-$3p$ states in substoichiometric $Si_3N_{4-x}$, whereas N related lone pair states dominate in stoichiometric $Si_3N_4$. The other notable observation is that the Fermi level is pushed upwards by 0.5 eV, as the stoichiometry changes from $Si_3N_4$ to $Si_3N_3$, in agreement with the less electronegative character of Si. Again we stress that we have aligned the electronic DOS at the N $1s$ core level, but this seems to be a rather sensible approach, since the local coordination of the N atoms remains virtually unchanged from $Si_3N_4$ to $Si_3N_3$.

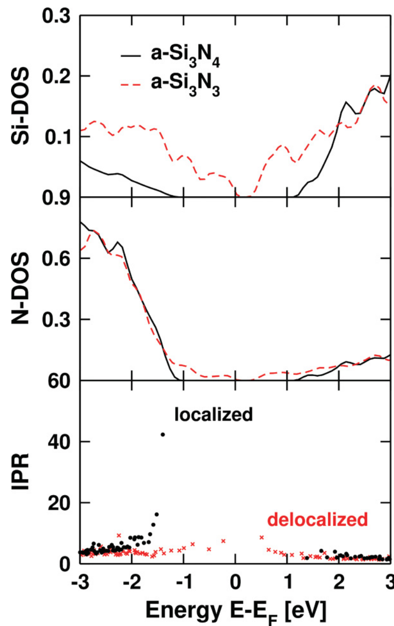


FIG. 12. (Color online) Density of states projected onto Si and N atoms and the inverse participation ration (IPR) for a-$Si_3N_3$ (red) and a-$Si_3N_4$ (black).

### B. Inverse participation ratio

It is commonly expected that the inverse participation ratio (IPR) increases for states in the gap (see, e.g., Justo *et al.*).[19] In the present case, we show the results only for the large systems, because the values for the small systems remain more bounded. The IPR is calculated as

$$p_n^{-1} = \frac{N \sum_{j,l} |\psi_{n,l}(\mathbf{r}_j)|^4}{(\sum_{j,l} |\psi_{n,l}(\mathbf{r}_j)|^2)^2}, \tag{6}$$

where $\psi_{n,l}(r_j)$ is the projection of the orbital $n$ onto the atomic site $j$ and angular quantum number $l$. The sum is performed over all atoms $j$ and the angular momentums $l$, whereas $N$ is the total number of atoms. If all atoms participate in an electronic state $n$, $p_n^{-1}$ becomes equal to 1, and, if the state is completely localized on one atom, $p_n^{-1}$ approaches $N$.

Figure 12 shows the partial (N and Si) resolved DOS and the IPR for a-$Si_3N_4$ and a-$Si_3N_3$. For stoichiometric a-$Si_3N_4$, we found very localized states at the valance-band edge and a DFT band gap of about 2 eV. Furthermore, for the considered snapshot no defect states are visible in the gap, in agreement with results of Giacomazzi and Umari.[23] As discussed above, the band gap becomes smaller and the DOS increases close to

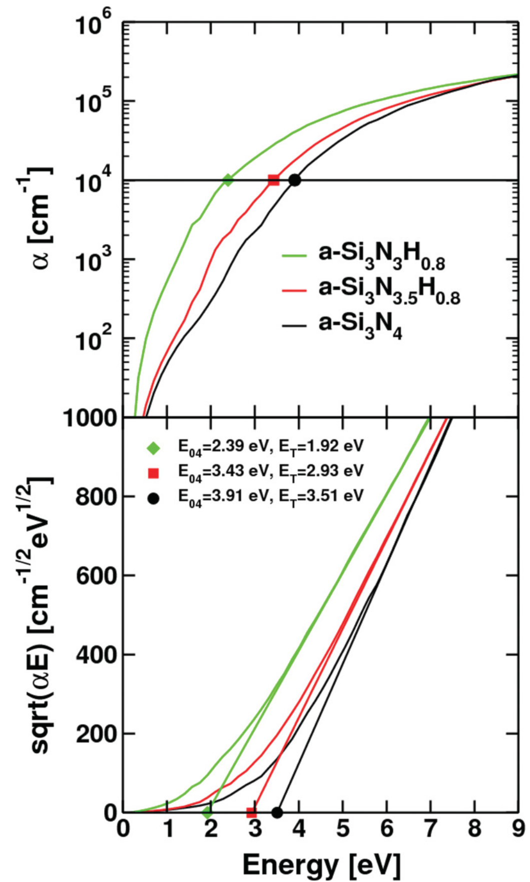


FIG. 13. (Color online) Optical band gap of $Si_3N_xH_y$ from density functional theory estimated by applying a threshold of $10^4$ cm$^{-1}$ to the absorption coefficient $\alpha$ and by using the Tauc linear regression (Ref. 52). The bisections give the corresponding results $E_{04}$ and $E_T$. To compare with experiment the DFT data need to be blueshifted to account for quasiparticle corrections (compare Table V).

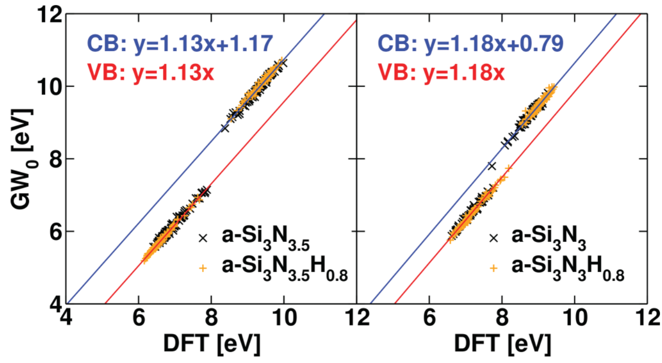


FIG. 14. (Color online) The eigenvalues of the highest occupied and lowest unoccupied orbitals for DFT and $GW_0$ calculations. The latter opens a gap of 1.17 and 0.79 eV between lowest occupied and highest unoccupied orbital, and increases the slope.

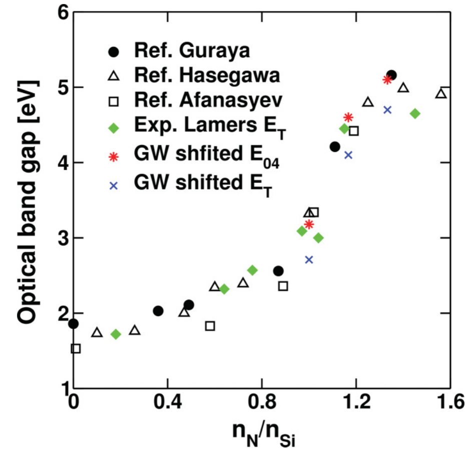


FIG. 15. (Color online) Comparison of calculated optical band-gap values (see Fig. 13) with experimental reference values (Refs. 6, 60, and 61). As described in the text, the calculated values are shifted by a corresponding $GW_0$ correction (compare Fig. 14 and Table V).

the Fermi level when moving off stoichiometry, in particular, the Si DOS increases around the Fermi level, in accordance with the observations made already in the previous section. It is also clearly visible that this results in much weaker localization and smaller IPR values for the states at the valence- and conduction-band edges as well as in the band gap.

### C. Optical band gap

A three-step procedure following roughly the experimental methods is used to determine the optical band gap: In the first step, we calculated the absorption coefficient $\alpha(E)$ from the independent particle dielectric function calculated using density functional theory orbitals and one-electron energies.[49–51]

Second, we determine the DFT optical band gap either as $E_{04}$, the energy value where the absorption coefficient $\alpha$ reaches the threshold of $10^4$ cm$^{-1}$, or as the Tauc band gap $E_T$ where the linear regression of the linear regime of $\sqrt{\alpha E}$ crosses the energy axis. In our case the linear regime is between 6 and 9 eV. The corresponding data are shown in Fig. 13 and are explained in more detail by Robertson, Zanatta, and Chambouleyron, and by Tauc.[12,52,53]

Finally, we applied the $GW_0$ approximation[54–57] to a set of 40 representative slowly cooled samples for each stoichiometry in order to correct the DFT band gaps which are well known to underestimate experimental quasiparticle band gaps. The $GW_0$ calculations were performed by iterating the eigenvalues in the Green's function until self-consistency was reached,[58,59] whereas the orbitals were kept fixed to the Kohn-Sham orbitals. We included typically 3500 unoccupied states, and one calculation required about 2 h on 64 cores.

TABLE V. Parameter obtained by fitting the linear function $y = kx + \Delta$ to the $GW_0$ quasiparticle energies as a function of the DFT one-electron energies for a-$Si_3N_xH_y$ (compare Fig. 14). The scissor correction $\Delta$ is added to the optical DFT band-gap values determined in Fig. 13.

| | $Si_3N_3H_{0\backslash 0.8}$ | $Si_3N_{3.5}H_{0\backslash 0.8}$ | $Si_3N_4$ |
|---|---|---|---|
| $k$ | 1.18 | 1.13 | 1.12 |
| $\Delta$ | 0.79 eV | 1.17 eV | 1.19 eV |

Doubling the number of unoccupied orbitals increased the quasiparticle band gap by less than 100 meV. The calculational details are otherwise similar to Ref. 48.

Figure 14 shows that the unoccupied states of $Si_3N_{3.5}$, with and without hydrogen, are rigidly shifted upwards by 1.17 eV compared to the occupied states. Furthermore, in the vicinity of the gap the $GW_0$ quasiparticle energies exhibit a slightly increased slope compared to the DFT one-electron energies. This slope is almost constant for the valence-band and conduction-band states and amounts 1.13. Disregarding the corrections for the slope, we can simply add an optical band-gap correction of $\Delta = 1.17$ eV to the DFT values $E_{04}$ and $E_T$. The scissor gap corrections $\Delta$ for the other stoichiometries are summarized in Table V.

In Fig. 15, we compare the corrected data of $E_{04}$ and $E_T$ with the experimental results obtained by Guraya *et al.*[6] As one can see, the values of $E_{04}$ are generally greater than $E_T$, but both lie only slightly below the experimental reference and follow the experimental data quite well. We note in particular the sharp decrease of the band gap, when one approaches the stoichiometry of $Si_3N_3$, which is a result of the increasing number of Si-Si bonds and the resultant percolation network accompanied by a change of the valence-band states from N lone pair to Si-Si bonding linear combinations (compare Fig. 11). In passing, we note that a scissor correction will not modify the density of states presented in Fig. 11, but for a trivial upshift of the conduction-band states and an opening of the gap between the valence-band and conduction-band states.

## V. CONCLUSIONS

This work presents a detailed study of a-$Si_3N_{4-x}$:H using periodic *ab initio* density functional theory calculations. Preparation of the samples proceeded via cooling from the melt using *ab initio* molecular dynamics. We have chosen this approach in order to avoid a mismatch between the creation of the model structures and evaluation of the electronic properties, since we expect the structural and electronic properties to be strongly intermingled, in particular, at defect sites. Conventional pair

or many-body potentials often have difficulties to describe this relation, as they necessarily cannot account for the introduced electronic defect states or the charge state of a defect.

As already emphasized from the outset, the present study concentrates on the "average" structural properties, paying little attention to details such as the defect concentration and electronic defect states in and close to the band gap. This is left for future studies, although the structural models determined in this work are expected to form a reliable basis for the subsequent studies.

We have shown that the average structural properties and electronic properties are faithfully reproduced using fairly small ensembles containing only 100 atoms. Using soft potentials with a plane-wave cutoff energy of 150 eV (resulting in typically 40–50 plane waves per atom), we were able to perform calculations for up to 1 ns with reasonably modest computational resources. For each considered stoichiometry, amorphous model structures were prepared by rapidly quenching about 1000 structures from the molecular dynamics simulation into the closest local minimum. We compared these structural models with larger calculations performed for systems with 200 atoms, and the results were found to be essentially identical for the small and large systems.

Analysis of the structural properties reveals that amorphous $Si_3N_x$ is characterized by fourfold coordinated Si atoms and threefold coordinated N atoms, with a very strong tendency towards heterocoordination and formation of Si-N bonds. Si-Si and N-N bonds are only encountered if a Si or N surplus, respectively, exists, but even then almost all Si and N atoms maintain their fourfold and threefold coordination, respectively.

For $Si_3N_3$, the structure factor shows the onset of density fluctuations in the N concentration, indicating N rich and N poor areas in the simulation cells. This observation in reciprocal space was also confirmed by the analysis of the local bonding properties of Si atoms. A clear fingerprint for clustering is the increased number of Si atoms with three Si neighbors in $Si_3N_{3.5}$ and the existence of Si atoms with four Si neighbors in $Si_3N_3$, which would not be expected if the formation of Si-Si bonds were entirely random. We, however, note that the tendency towards clustering is not overwhelmingly strong in agreement with experiments where no sign of phase separation is found.

The evolution of the electronic properties of $Si_3N_{4-x}$ is quite remarkable. In the stoichiometric compound, the valence-band maximum is dominated by N lone pair states, whereas the valence-band minimum is dominated by antibonding Si $p$ states. However, this changes as the N content decreases. For substoichiometric samples, some Si atoms need to bond to other Si atoms and at a critical stoichiometry of $Si_3N_3$ about 20% of the Si atoms have two or more Si neighbors. Concomitantly, Si-Si-Si chains and larger percolation networks start to form, and about 60% of the Si atoms are found in such percolation networks at the stoichiometry $Si_3N_3$. Within a Si pair, but even more so within a Si chain, the bonding-antibonding splitting is reduced compared to a Si-N bond, and hence the valence-band edge becomes progressively dominated by Si-Si bonding contributions. Likewise the conduction-band edge becomes dominated by states originating from Si pairs in $Si_3N_{3.5}$ and chains in $Si_3N_3$. We finally note that with decreasing N content the localization of the band edge states at the valence- and conduction-band edges decreases. This is in accordance with the picture developed above: as the Si chain size increases, the states will start to spread over the Si chain with a resultant reduced inverse participation ratio. In agreement with experiment, we also find that the band gap reduces slightly from $Si_3N_4$ to $Si_3N_{3.5}$, but it shows a sharp decrease for $Si_3N_3$ as the chain size grows. We note that in stoichiometric $Si_3N_4$ the valence band is entirely dominated by N lone pair states, and hence stoichiometric $Si_3N_4$ is not suitable to model the electronic properties of passivation layers in solar cells used by industry.

Finally, we have analyzed the impact of hydrogen on silicon nitrides in detail. Remarkably, it has no visible impact on the averaged properties such as the pair-correlation function, the structure factor, or the electronic density of states. In agreement with common chemical intuition, we have, however, noticed that hydrogen can attach to a N or Si atom terminating a dangling bond. This is in accordance with the commonly accepted picture that H helps to reduce the number of electronic defect states in the gap, although a more careful analysis of the electronic properties of defects is required to fully resolve this issue.

## ACKNOWLEDGMENT

This work is part of the HiperSol project (High Performance Solar Cells) funded by European Commission Grant No. MMP3-SL-2009-228513. We thank the project members for their support and inspiring discussions.

[1] F. Duerinckx and J. Szlufcik, Sol. Energy Mater. Sol. Cells **72**, 231 (2002).
[2] W. Soppe, H. Rieffe, and A. Weeber, Prog. Photovoltaics **13**, 551 (2005).
[3] F. Giorgis, C. F. Pirri, and E. Tresso, Thin Solid Films **307**, 298 (1997).
[4] F. Giorgis, F. Giuliani, C. F. Pirri, E. Tresso, C. Summonte, R. Rizzoli, R. Galloni, A. Desalvo, and P. Rava, Philos. Mag. B **77**, 925 (1998).
[5] C. J. Mogab and E. Lugujjo, J. Appl. Phys. **47**, 1302 (1976).
[6] M. M. Guraya, H. Ascolani, G. Zampieri, J. I. Cisneros, J. H. Dias da Silva, and M. P. Cantão, Phys. Rev. B **42**, 5677 (1990).
[7] T. Aiyama, T. Fukunaga, K. Niihara, T. Hirai, and K. Suzuki, J. Non-Cryst. Solids **33**, 131 (1979).
[8] M. Misawa, T. Fukunaga, K. Niihara, T. Hirai, and K. Suzuki, J. Non-Cryst. Solids **34**, 313 (1979).
[9] P. M. Lenahan and S. E. Curry, Appl. Phys. Lett. **56**, 157 (1990).
[10] W. L. Warren, P. M. Lenahan, and S. E. Curry, Phys. Rev. Lett. **65**, 207 (1990).
[11] J. Robertson and M. J. Powell, Appl. Phys. Lett. **44**, 415 (1984).

[12]J. Robertson, Philos. Mag. B **63**, 47 (1991).
[13]J. Robertson, Philos. Mag. B **69**, 307 (1994).
[14]J. Robertson, W. Warren, and J. Kanicki, J. Non-Cryst. Solids **187**, 297 (1995).
[15]N. Umesaki, N. Hirosaki, and K. Hirao, J. Non-Cryst. Solids **150**, 120 (1992).
[16]L. Ouyang and W. Y. Ching, Phys. Rev. B **54**, R15594 (1996).
[17]F. De Brito Mota, J. F. Justo, and A. Fazzio, Int. J. Quantum Chem. **70**, 973 (1998).
[18]F. de Brito Mota, J. F. Justo, and A. Fazzio, J. Appl. Phys. **86**, 1843 (1999).
[19]J. F. Justo, F. de Brito Mota, and A. Fazzio, Phys. Rev. B **65**, 073202 (2002).
[20]F. Alvarez and A. A. Valladares, Phys. Rev. B **68**, 205203 (2003).
[21]S. Y. Lin, Opt. Mater. **23**, 93 (2003).
[22]S. Z. Karazhanov, P. Kroll, A. Holt, A. Bentzen, and A. Ulyashin, J. Appl. Phys. **106**, 053717 (2009).
[23]L. Giacomazzi and P. Umari, Phys. Rev. B **80**, 144201 (2009).
[24]K. Jarolimek, R. A. de Groot, G. A. de Wijs, and M. Zeman, Phys. Rev. B **82**, 205201 (2010).
[25]M. Ippolito and S. Meloni, Phys. Rev. B **83**, 165209 (2011).
[26]S. Nekrashevich, A. Shaposhnikov, and V. Gritsenko, JETP Lett. **94**, 202 (2011).
[27]E. C. Ferreira and C. E. T. Gonçalves da Silva, Phys. Rev. B **32**, 8332 (1985).
[28]P. Kroll, J. Non-Cryst. Solids **293**, 238 (2001).
[29]R. P. Vedula, N. L. Anderson, and A. Strachan, Phys. Rev. B **85**, 205209 (2012).
[30]T. M. Searle, *Properties of Amorphous Silicon and its Alloys* (INSPEC, The Institution of Electrical Engineers, London, UK, 1998).
[31]R. E. I. Schropp, S. Nishizaki, Z. Houweling, V. Verlaan, C. van der Werf, and H. Matsumura, Solid-State Electron. **52**, 427 (2008).
[32]N. W. Ashcroft and N. D. Mermin, *Solid State Physics* (Brooks-Cole, Belmont, MA, 1976).
[33]A. R. Denton and N. W. Ashcroft, Phys. Rev. A **43**, 3161 (1991).
[34]E. Bustarret, M. Bensouda, M. C. Habrard, J. C. Bruyère, S. Poulin, and S. C. Gujrathi, Phys. Rev. B **38**, 8171 (1988).
[35]P. E. Blöchl, Phys. Rev. B **50**, 17953 (1994).
[36]J. Furthmüller, J. Hafner, and G. Kresse, Phys. Rev. B **50**, 15606 (1994).
[37]G. Kresse and J. Furthmüller, Phys. Rev. B **54**, 11169 (1996).
[38]G. Kresse and D. Joubert, Phys. Rev. B **59**, 1758 (1999).
[39]J. P. Perdew, A. Ruzsinszky, G. I. Csonka, O. A. Vydrov, G. E. Scuseria, L. A. Constantin, X. Zhou, and K. Burke, Phys. Rev. Lett. **100**, 136406 (2008).
[40]R. Riedel and M. Seher, J. Eur. Ceram. Soc. **7**, 21 (1991).
[41]Y. Cerenius, J. Am. Ceram. Soc. **82**, 380 (1999).
[42]S. Garcia, D. Bravo, M. Fernandez, I. Martil, and F. J. López, Appl. Phys. Lett. **67**, 3263 (1995).
[43]K. Jarolimek, R. A. de Groot, G. A. de Wijs, and M. Zeman, Phys. Rev. B **79**, 155206 (2009).
[44]T. E. Faber and J. M. Ziman, Philos. Mag. **11**, 153 (1965).
[45]N. W. Ashcroft and D. C. Langreth, Phys. Rev. **156**, 685 (1967).
[46]P. Vashishta, R. K. Kalia, J. P. Rino, and I. Ebbsjö, Phys. Rev. B **41**, 12197 (1990).
[47]J. P. Hansen and I. R. McDonald, *Theory of Simple Liquids*, 3rd ed. (Elsevier, Amsterdam, The Netherlands, 2006).
[48]G. Kresse, M. Marsman, L. E. Hintzsche, and E. Flage-Larsen, Phys. Rev. B **85**, 045205 (2012).
[49]E. D. Palik, *Handbook of Optical Constants of Solids*, Vol. 3 (Academic, San Diego, USA, 1998).
[50]M. P. Prange, J. J. Rehr, G. Rivas, J. J. Kas, and J. W. Lawson, Phys. Rev. B **80**, 155110 (2009).
[51]M. Gajdoš, K. Hummer, G. Kresse, J. Furthmüller, and F. Bechstedt, Phys. Rev. B **73**, 045112 (2006).
[52]J. Tauc, Mater. Res. Bull. **5**, 721 (1970).
[53]A. R. Zanatta and I. Chambouleyron, Phys. Rev. B **53**, 3833 (1996).
[54]L. Hedin, Phys. Rev. **139**, A796 (1965).
[55]M. S. Hybertsen and S. G. Louie, Phys. Rev. B **34**, 5390 (1986).
[56]W. G. Aulbur, L. Jönsson, and J. W. Wilkins, in *Solid State Physics*, Vol. 54 (Academic, San Diego, USA, 2000), pp. 1–218.
[57]F. Aryasetiawan and O. Gunnarsson, Rep. Prog. Phys. **61**, 237 (1998).
[58]M. Shishkin and G. Kresse, Phys. Rev. B **74**, 035101 (2006).
[59]M. Shishkin and G. Kresse, Phys. Rev. B **75**, 235102 (2007).
[60]S. Hasegawa, M. Matsuda, and Y. Kurata, Appl. Phys. Lett. **58**, 741 (1991).
[61]I. V. Afanasyev-Charkin, L. G. Jacobsohn, R. D. Averitt, and M. Nastasi, J. Vac. Sci. Technol. A **22**, 2342 (2004).